2014 IEEE International Conference on Robotics & Automation (ICRA)
Hong Kong Convention and Exhibition Center
May 31 - June 7, 2014. Hong Kong, China

Planar Multi-Contact Bipedal Walking Using Hybrid Zero Dynamics

Jordan Lack, Matthew J. Powell, and Aaron D. Ames

***Abstract*— This paper presents a method for achieving planar multi-phase, multi-contact robotic walking using human inspired control and optimization. The walking presented contains phases with differing degrees of actuation including over-actuated double support, fully-actuated single support, and under-actuated single support via heel lift. An optimization methodology for generating walking gaits using partial hybrid zero dynamics will be presented. It will be shown that this method yields periodic, multi-contact locomotion. Simulation results for the three domain walking under standard Input-Output Linearization control will be presented.**

I. INTRODUCTION

Human walking consists of multiple phases, referred to in this paper as domains, including instances of single support and double support that together result in efficient, fluid locomotion. Between these domains are transition events such as heel strike, toe strike, toe off, and heel off that allow humans to elegantly regulate gait characteristics such as walking speed, step length, and step frequency. With the goal of designing robust and efficient robotic walking, it is essential that control theorists strive to develop walking controllers capable of taking advantage of these same gait characteristics. Unfortunately, the overwhelming majority of robotic walking to date revolves around the assumption that the feet are flat and remain flat throughout the gait, which greatly reduces the ability to walk efficiently.

Though flat footed walking is less efficient, countless methods have been developed and realized on robots that have worked well and have been demonstrated to be surprisingly robust. One of the most widely used approaches is to design walking controllers around the zero moment point (ZMP) [9], [24]. The ZMP approach has been successfull in producing surprisingly robust locomotion on a number of humanoid platforms including Honda's ASIMO [14], the entire series of HRP humanoids from Kawada Industries (see HRP-2 in [23]), as well as countless other humanoid robots (see [8] for another example).

Another control strategy similar to ZMP based control is capture point control [11], [16]. Capture point control is based upon finding regions on the stepping surface in which the robots state is capturable, meaning the robot can successfully stop. Capture point has been successfully realized experimentally on the humanoid M2V2 [17] with both walking and push recovery. Other more mathematically formal methods that have been developed more recently include geometric reduction [6], [20], control symmetries [21], and hybrid zero dynamics [2], [6]. Hybrid zero dynamics based control has seen great success on multiple platforms such as RABBIT [5], MABEL [22], ATRIAS [7], AMBER 1 [18], and AMBER 2 [15]. Extraordinarily, MABEL has also achieved human-like running using hybrid zero dynamics based control [22].

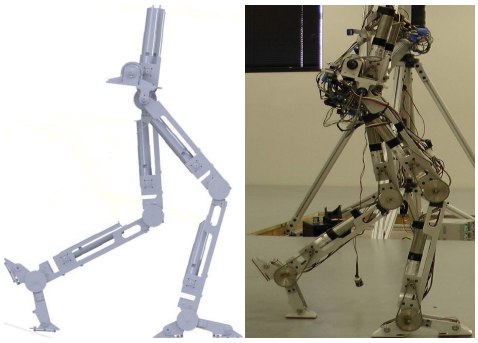

Fig. 1: Bipedal robotic testbed AMBER 2 seen on the left in a SolidWorks rendering and on the right as the robot is today.

In this paper, a human-inspired optimization will be presented that yields controller parameters defining parameterized reference trajectories for a three domain walking gait consisting of all the key phases of human-like walking: over-actuation, full-actuation, and under-actuation. The robot model used is that of AMBER 2 pictured in Fig. 1, the footed successor to AMBER 1. The remainder of this paper will be structured as follows: Section II defines the multi-domain hybrid system model and discusses contact conditions and actuation types. Section III introduces human inspired control. Section IV introduces partial hybrid zero dynamics (PHZD) and highlights the properties of PHZD useful for walking gait construction. Section V describes the main result of this paper: construction of a multi-domain, human-inspired optimization. Section VI provides simulation results and a discussion on the proposed method.

II. HYBRID CONTROL SYSTEM MODEL

This section develops the mathematical model for multi-contact locomotion for a bipedal robot with feet. In particular, the changing of contact points over a walking gait, e.g., lifting and striking of the heel and toe, necessitates a model of the robot that includes continuous and discrete dynamics. For this paper the goal will be to construct a walking gait

Jordan Lack, Matthew J. Powell and Aaron D. Ames are with the Department of Mechanical Engineering, Texas A&M University, College Station, TX 77843.
jlack1987@gmail.com, {mjpowell,aames}@tamu.edu

This research is supported by NASA grants NNX11AN06H and NNX12AQ68G, NSF grants CPS-1239085, CNS-0953823 and CNS-1136104, and the Texas Emerging Technology Fund.

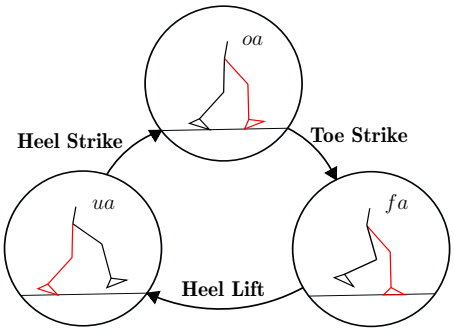

Fig. 2: Directed graph associated with 3 domain walking. The stance leg is red and non-stance leg is black.

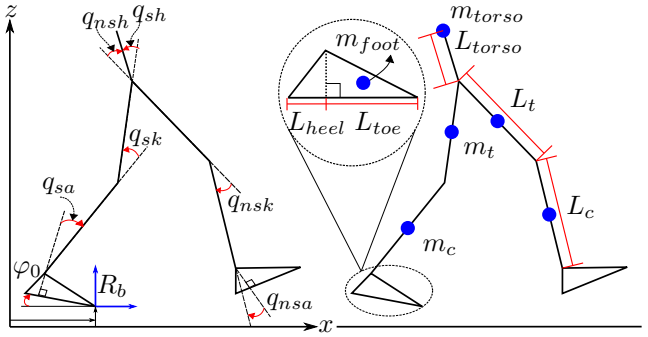

Fig. 3: Coordinates of 9 degree of freedom footed biped model (left) and layout of physical parameters (right).

consisting of three discrete domains (see Fig. 2).

Hybrid System Model. The formal model of a bipedal robot with a multi-contact multi-domain walking gait follows the general development given in [12], [19]. In particular, we consider a *hybrid control system model* given by a tuple:

$$\mathscr{HC} = (\Gamma, D, U, S, \Delta, FG), \tag{1}$$

where $\Gamma = (V, E)$ is a directed graph with vertices and edges. For $v \in V$ and $e \in E$, $D = \{D_v\}$ is a set of domains, $U = \mathbb{R}^{m_r}$ is a set of admissible controls, $S = \{S_v\}$ is a set of guards, $\Delta = \{\Delta_e\}$ is a set of transition maps, and $FG = \{FG_v\}$ is a set of control systems. These elements are discussed in more detail in the following sections.

Three-Domain Graph. For the multi-contact walking gait of interest, the graph Γ of the hybrid system $\mathscr{HC}$ is pictured in Fig. 2. In particular, Γ is a directed cycle, with a set of vertices, V, and a set of edges, E, given by:

$$V = \{\text{oa}, \text{fa}, \text{ua}\}, \tag{2}$$
$$E = \{e_{\text{ts}} = (\text{oa} \to \text{fa}), e_{\text{hl}} = (\text{fa} \to \text{ua}), e_{\text{hs}} = (\text{ua} \to \text{oa})\},$$

where in this case, we have labeled each vertex $v \in V$ (which is used to index a domain D_v) by the type of actuation in the corresponding domain (as will be discussed later), i.e., the vertices oa, fa and ua correspond to over, full and under actuation, respectively. Associated with each edge in the graph, $e = (v \to v') \in E$, is a transition map Δ_e from the one domain to the next, i.e. $\Delta_e : D_v \to D_{v'}$.

Coordinates, Constraints and Actuation Types. The generalized configuration space for the chosen robot model is $Q = \mathbb{R}^2 \times SO(2) \times Q_r$ where Q_r is characterized by the relative joint angles (see Fig 3); specifically, the (generalized) coordinates are given by $q = \{p_x, p_z, \varphi_0, q_r\}$ where $q_r = \{q_{sa}, q_{sk}, q_{sh}, q_{nsh}, q_{nsk}, q_{nsa}\}$ and $\{p_x, p_z, \varphi_0\}$ reference the body fixed frame R_b with respect to a fixed inertial frame R_0 shown in Fig. 3.

Contact Conditions: For each vertex of the graph Γ, there are associated contact points interacting with the physical world that dictate multi-contact conditions in the robot [4]. This is represented by a set of contact points $\mathcal{C}_v \subset \{sh, st, nsh, nst\}$, where sh is the stance-heel, st is the stance-toe, nsh is the non-stance heel and nst is the non-stance toe. With this, we consider two types of constraints: *unilateral*, denoted h_v, and *holonomic*, denoted η_v. Unilateral constraints dictate the set of admissible states, while holonomic constraints are used to encode which points are in contact with the walking surface.

Example 1: For the domain structure considered in this paper (see Fig. 2) there are the following constraints:

- For $v = \text{fa} \in V$, $h_{\text{fa}}(q)$ consists of the z position of the non-stance heel, and $\eta_{\text{fa}}(q)$ consists of the x, z position of the stance toe together with the z position of the stance heel.
- For $v = \text{ua} \in V$, $h_{\text{ua}}(q)$ consists of the z position of the non-stance heel, while $\eta_{\text{ua}}(q)$ consists of the x, z position of the stance toe.
- For $v = \text{oa} \in V$, $h_{\text{oa}}(q)$ consists of the z position of the stance toe, while $\eta_{\text{oa}}(q)$ consists of the x, z positions of the stance heel and non-stance toe.

Actuation Type: For a given robot, let m_r denote the number of actuators, let n denote the number of unconstrained degrees of freedom, let n_{c_v} denote the number of holonomic constraints in a given domain, and let $n_v = n - n_{c_v}$ denote the number of constrained degrees of freedom in a given domain, v. We say that a domain is

- *Fully-actuated* if $m_r = n - n_{c_v}$,
- *Under-actuated* if $m_r < n - n_{c_v}$,
- *Over-actuated* if $m_r > n - n_{c_v}$.

Understanding and managing these three types of actuation is an important aspect of this paper; the actuation type affects both the dynamics of the robot and the permissible control.

Example 2: AMBER 2 has six actuators, thus $m_r = 6$ and $n = 9$. For $\text{oa} \in V$, $n_{c_{\text{oa}}} = 4$ thus $n - n_{c_{\text{oa}}} = 9 - 4 = 5 < 6$ and the robot is over-actuated in oa. For fa, $n_{c_{\text{fa}}} = 3$ thus $n - n_{c_{\text{fa}}} = 9 - 3 = 6$ and therefore the robot is fully-actuated in fa. For ua, $n_{c_{\text{ua}}} = 2$ thus $n - n_{c_{\text{ua}}} = 9 - 2 = 7 > 6$ and therefore the robot is under-actuated in ua.

Control System. We now have the necessary framework in which to construct the control system FG_v for each domain of the hybrid system $\mathscr{HC}$ given in (1). In particular, the control system on each domain will be obtained from general "unpinned" dynamics subject to holonomic constraints corresponding to forceful nature of the interaction between the

robot and the environment; see [6] for a detailed derivation. The resulting constrained dynamical system is described by,

$$M(q)\ddot{q} + C(q,\dot{q})\dot{q} + G(q) = B(q)u + J_v(q)^T F_v, \quad (3)$$

where $M(q)$, $C(q,\dot{q})$ and $G(q)$ are the inertia matrix, Coriolis matrix, and gravity vector, respectively, B determines the distribution of joint torques, $u \in \mathbb{R}^{m_r}$, and F_v is the contact *wrench* containing reaction forces and moments [6]. Let $x := (q, \dot{q})$ so that (3) can be written

$$\dot{x} = f_v(x) + g_v(x)u, \qquad v \in V, \quad (4)$$

where the methods described in [6] are used to express the wrench, F_v, as a function of the joint states and joint torques. Thus the control system on v is $FG_v = (f_v, g_v)$.

Domains, Guards and Reset Maps. A continuous domain is the set of admissible configurations of the system, as dictated by contact constraints. Specifically, one can ensure that the foot does not slip or rotate by considering inequalities of the form: $\mu_v(q)^T F_v(q,\dot{q},u) \geq 0$, with μ_v a matrix of friction parameters (see [19] for more details). Coupled with the unilateral constraints, $h_v(q)$, the constraints on the domain are,

$$\Psi_v(q,\dot{q},u) = \begin{bmatrix} \mu_v(q)^T F_v(q,\dot{q},u) \\ h_v(q) \end{bmatrix} \geq 0. \quad (5)$$

The continuous domain is thus given by:

$$D_v = \{(q,\dot{q},u) \in TQ \times \mathbb{R}^{m_r} : \Psi_v(q,\dot{q},u) \geq 0\}. \quad (6)$$

The guard is just the boundary of this domain with the additional assumption that the set of admissible configurations is decreasing, i.e. the vector field is pointed outside of the domain:

$$S_v = \{(q,\dot{q},u) \in TQ \times \mathbb{R}^{m_r} : \Psi_v(q,\dot{q},u) = 0, \quad (7)$$
$$\dot{\Psi}_v(q,\dot{q},u) < 0\}. \quad (8)$$

The transition map for an edge $e = (v \to v')$ is given by:

$$\Delta_e : S_v \to D_{v'}, \qquad \Delta_e(q,\dot{q}) = \begin{bmatrix} \Delta_q q \\ \Delta_q P_e \dot{q} \end{bmatrix}, \quad (9)$$

where Δ_q is a relabeling matrix[1], and P_e is computed from impact equations assuming perfectly plastic impacts (see [25]) and no slipping. Note that the reset map from full to under-actuation is the identity map as no impact occurs.

III. Multi-Domain Human-Inspired Control

This section extends the framework of human-inspired control [2] to the multi-contact case, i.e., the case where there are multiple discrete domains. In particular, it is necessary to consider phases of under, over and full actuation. This general construction, applicable to general mixed actuation gaits, will be specialized the case of AMBER 2 for the discrete structure given in Fig. 2.

[1]Note that as a result of considering "stance" and "non-stance" legs, the labeling on the legs must be switching during one of the transitions; in this paper, these switching occurs at heel strike. This is a common "trick" in robotic walking used to reduce the number of discrete domains.

Consider the following system defined on each domain $v \in V$:

$$\dot{x} = f_v(x) + g_v(x)u, \quad (10)$$
$$y_v = y_v^a(x) - y_v^d(x), \quad (11)$$

for $x \in D_v$ and $u \in U_v$ and where y_v is a *control output* for $v \in V$, consisting of the difference between an actual output $y_v^a(x)$ and a desired value for this output $y_v^d(x)$. The human-inspired control design process consists of proper choice of actual and desired outputs, along with construction of a control law $u(q,\dot{q})$ that drives $y_v^a(x) \to y_v^d(x)$ such that the resulting hybrid system obtained by applying this control law has a periodic orbit, i.e., a walking gait.

Human Locomotion (Actual) Outputs. Motivated by the consideration of human locomotion data in previous work [4], we will construct actual outputs, y_v^a, through the use of human output combinations [1]. The human outputs of interest here include both the stance and non-stance knee angles, the angle between the hips, the angle of the non-stance foot with the ground, the angle of the robots torso, and the stance ankle angle. It has been shown through the analysis of human walking data [4] that these outputs behave in a simple manner and can be represented with functions that are *linear* combinations of the robots joint angles.

Definition 1: A human output combination for $v \in V$ is a tuple $Y_v^H = (Q_r, y_{1,v}^H, y_{2,v}^H)$ consisting of a configuration space Q_r, a velocity-modulating output $y_{1,v}^H(q)$ and position-modulating outputs $y_{2,v}^H(q)$. Let O_v be an indexing set for $y_{2,v}^H$ whereby $y_{2,v}^H(q) = [y_{2,v}^H(q)_o]_{o \in O_v}$. A set of human outputs are *independent* if,

$$\text{rank}\left(\begin{bmatrix} y_{1,v}^H(q) \\ y_{2,v}^H(q) \end{bmatrix}\right) = n_v, \quad (12)$$

on Q_r, and *linear* if

$$y_{1,v}^H(q) = c_v q, \quad (13)$$
$$y_{2,v}^H(q) = H_v q, \quad (14)$$

for $c_v \in \mathbb{R}^{1 \times n_v}$ and $H_v \in \mathbb{R}^{(n_v-1)\times n_v}$.

Example 3: We choose the following linear and independent human output combinations for the three domains of interest. For the velocity modulating output, we consider the same linear output for all three domains characterized by:

$$c_v = \begin{bmatrix} 0 & 0 & 0 & -L_c - L_t & -L_t & 0 & 0 & 0 & 0 \end{bmatrix}, \quad (15)$$

for $v \in V = \{\text{oa}, \text{fa}, \text{ua}\}$, with L_c the length of the calf and L_t the length of the thigh of the robot. The velocity modulating output $y_{1,v}^H(q)$ is simply the linearized forward position of the hip. For the position modulating outputs, we first consider the linear outputs for the under-actuated domain characterized by

$$H_{\text{ua}} = \begin{bmatrix} 0 & 0 & 0 & 1 & 0 & 0 & 0 & 0 & 0 \\ 0 & 0 & 0 & 0 & 1 & 0 & 0 & 0 & 0 \\ 0 & 0 & 0 & 0 & 0 & 0 & 0 & 1 & 0 \\ 0 & 0 & 0 & 0 & 0 & 1 & -1 & 0 & 0 \\ 0 & 0 & 1 & 1 & 1 & 1 & 0 & 0 & 0 \\ 0 & 0 & 1 & 1 & 1 & 1 & -1 & -1 & -1 \end{bmatrix}. \quad (16)$$

The position modulating outputs for the over- and fully-actuated domains are chosen to be submatrices of H_{ua} based upon the available degrees of actuation in these respective domains. In particular, $H_{\text{oa}} = (H_{\text{ua}})_{1,2,5,6}$ and $H_{\text{fa}} = (H_{\text{ua}})_{2-6}$, where here we have used the notation $(H_{\text{ua}})_i$ to denote the i^{th} row of H_{ua}. Note that this is not the only valid choice of human output combination, but the one chosen here based upon examination of human locomotion data.

Canonical Walking Functions. Previous results [4] reveal that for the actual outputs considered, humans tend to display very simple behavior. This observation motivates the use of simple desired functions for bipedal locomotion. In particular, it was observed [4] through examination of human walking data that the "proper" choice of the velocity modulating output satisfies the property that:

$$y^H_{1,v}(q) \approx v_{hip} t. \tag{17}$$

In addition, by selectively choosing the human outputs, they appear to be described by the solution to a linear mass-spring damper system. With this in mind, define the *canonical walking function*:

$$y_{\text{cwf}}(t, \alpha) = e^{-\alpha_4 t}(\alpha_1 \cos(\alpha_2 t) + \alpha_3 \sin(\alpha_2 t)) + \alpha_5. \tag{18}$$

Additionally, it was found that for more complex walking behavior, e.g., stair climbing and rough terrain locomotion [10], the position modulating outputs appear to be described by the solution to a linear mass-spring-damper system under sinusoidal excitation. With this in mind, define the *extended canonical walking function* (ECWF):

$$\begin{aligned} y_{\text{ecwf}}(t, \alpha) =& e^{-\alpha_4 t}(\alpha_1 \cos(\alpha_2 t) + \alpha_3 \sin(\alpha_2 t)) \\ &+ \alpha_5 \cos(\alpha_6 t) + \kappa(\alpha) \sin(\alpha_6 t) + \alpha_7, \end{aligned} \tag{19}$$

where $\kappa(\alpha) = (2\alpha_4\alpha_5\alpha_6)/((\alpha_2)^2+(\alpha_4)^2+(\alpha_6)^2)$. As found in [2] these functions represent (human) bipedal locomotion data with high correlation and therefore, we leverage these functions in construction of desired control outputs for bipedal locomotion and claim that the functions are natural suggestions for bipedal (human and robotic) walking.

Parameterization of Time. With these time-based functions in mind, and specifically (17), coupled with the desire to construct *autonomous* control functions, we specify the following *parameterization of time*:

$$\tau_v(q, \dot{q}) = \frac{y^H_{1,v}(q) - d_v}{v_{hip}} \tag{20}$$

where $y^H_{1,v}(q)$ is the velocity modulating output which, based upon the relationship in (17), is used to parameterize time and $d_v \in \mathbb{R}$ is used to align $\tau_v(q) = 0$ at critical points in the gait, i.e. at the start of specific domains $v \in V$.

Desired Output functions. With the goal of controlling the forward velocity of the robot, we define the relative degree one desired output to be:

$$y^d_{1,v} = v_{hip}, \qquad v \in V \tag{21}$$

for all domains, i.e., irrespective of actuation type. Similarly, with the goal of the robot tracking the canonical walking function, for the over-actuated domains, we define the desired outputs to be:

$$y^d_{2,v}(\tau_v(q), \alpha_v) = [y_{cwf}(\tau_v(q), \alpha^i_v)]_{i \in O_v}, \;\; v = oa \tag{22}$$

that is, for $v \in V$ s.t. $m_r > n - c_v$. Finally, in the case of either full or under-actuation, we define the desired output to be:

$$y^d_{2,v}(\tau_v(q), \alpha_v) = [y_{ecwf}(\tau_v(q), \alpha^i_v)]_{i \in O_v}, \;\; v \in \{fa, ua\} \tag{23}$$

that is, for $v \in V$ s.t. $m_r \leq n - n_{c_v}$. The change to the ECWF is needed for computing a Motion Transition (detailed reasoning will be given in Section IV).

Control Law Construction. The goal is to drive the outputs of the robot, obtained through a human output combination, to the outputs of the human as represented by the canonical walking functions parameterized by $\tau_v(q)$. This motivates the final form of the outputs, termed the *human-inspired outputs* and given by:

$$y_{1,v}(q, \dot{q}) = \dot{y}^H_{1,v}(q, \dot{q}) - v_{hip}, \tag{24}$$

$$y_{2,v}(q) = y^H_{2,v}(q) - y^d_{2,v}(\tau_v(q), \alpha_v). \tag{25}$$

From these outputs, we can construct two types of controllers: one for the fully and over-actuated domains, and one for the under-actuated domain. In the case of full and over-actuation, we define the *human-inspired controller* by:

$$\begin{aligned} u_v^{(\alpha_v, \varepsilon)}(q, \dot{q}) = -\mathcal{A}_v^{-1}(q) \Bigg(&\begin{bmatrix} 0 \\ L_{f_v} L_{f_v} y_{2,v}(q, \dot{q}) \end{bmatrix} \\ &+ \begin{bmatrix} L_{f_v} y_{1,v}(q, \dot{q}) \\ 2\varepsilon L_{f_v} y_{2,v}(q, \dot{q}) \end{bmatrix} + \begin{bmatrix} \varepsilon y_{1,v}(q, \dot{q}) \\ \varepsilon^2 y_{2,v}(q) \end{bmatrix} \Bigg), \end{aligned} \tag{26}$$

for $v \in \{fa, oa\}$. Here L is the Lie derivative, $\varepsilon > 0$ is a user defined control gain that dictates the convergence of $y_{1,v}$ and $y_{2,v}$ to 0, and

$$\mathcal{A}_v(q) = \begin{bmatrix} L_{g_v} y_{1,v}(q) \\ L_{g_v} L_{f_v} y_{2,v}(q) \end{bmatrix} \tag{27}$$

is the decoupling matrix. In a similar fashion, in the case of under-actuation, we define the human-inspired controller:

$$\begin{aligned} u_{ua}^{(\alpha_{ua}, \varepsilon)}(q, \dot{q}) = -\mathcal{A}_{ua}^{-1}(q) \big(&L_{f_{ua}} L_{f_{ua}} y_{2,ua}(q, \dot{q}) + \\ &2\varepsilon L_{f_{ua}} y_{2,ua}(q, \dot{q}) + \varepsilon^2 y_{2,ua}(q) \big) \end{aligned} \tag{28}$$

where in this case $\mathcal{A}_{ua} = L_{g_{ua}} L_{f_{ua}} y_{2,ua}(q)$. We note that $\mathcal{A}_v$ is assumed to non-singular for all $v \in V$ as a necessary condition for the human output combination Y^H_v to be valid; this also implies that $y_{1,v}$ and $y_{2,v}$ have the proper (vector) relative degree. Importantly, depending on the choice of outputs and constraints enforced, the control law (26) is a controller for the case of under, full and over actuation.

Applying the feedback control law in (26) and (28) to (4) yields dynamical systems for each domain. It is the behavior of this closed form system that we wish to analyze. In particular, the goal is to find parameters α_v for each domain such that a hybrid periodic orbit is generated for the closed form system. This is the aim of the human-inspired optimization problem that will be presented in the next section.

IV. Partial Hybrid Zero Dynamics

The optimization problem leverages the hybrid zero dynamics and partial hybrid zero dynamics concepts to produce low-dimensional representations of the system; this section introduces these concepts and corresponding notation. A *zero dynamics* surface $\mathcal{Z}_{\alpha_v}$ is defined by the set:

$$\mathcal{Z}_{\alpha_v} = \{(q, \dot{q}) \in Q : y_v(q, \dot{q}) = \mathbf{0}\}, \tag{29}$$

where $y_v(q, \dot{q})$ contains all relative degree one and/or two outputs and first time-derivatives of relative degree two outputs in the domain v. A *hybrid zero dynamics* [25], [1] is a zero dynamics surface that is invariant through impacts.

Properties of Partial Zero Dynamics. The definition of a partial zero dynamics (PZD) surface:

$$\mathcal{PZ}_{\alpha_v} = \{(q, \dot{q}) \in Q : y_2(q) = \mathbf{0}, \dot{y}_2(q, \dot{q}) = \mathbf{0}\}, \tag{30}$$

has two properties of interest that can be utilized in the construction of walking gaits. First, by definition, a PZD surface consists of equality constraints on the state space of the robot which can be combined with additional constraints to form a well-posed inverse kinematics problem.

In the over-actuated and fully-actuated domains, a second property associated with the PZD surface and the control law (26) is a "low-dimensional" (linear) dynamical system. Picking the coordinates $\xi_v = (\xi_{v,1}, \xi_{v,2})$, where $\xi_{v,1} := y^H_{1,v}(q)$ and $\xi_{v,2} := \dot{y}^H_{1,v}(q, \dot{q})$, and due to the specific choice of control law (26), the partial zero dynamics are given by:

$$\dot{\xi}_{v,1} = \xi_{v,2}, \tag{31}$$

$$\dot{\xi}_{v,2} = -\varepsilon(\xi_{v,2} - v_{hip}), \quad v \in \{oa, fa\}. \tag{32}$$

Let $\xi_v(t, \xi^+_v)$ be the solution to (31) and (32) with initial condition ξ^+_v; and note that because (31) and (32) describe a linear system, $\xi_v(t, \xi^+_v)$ can be obtained in closed form.

Obtaining States On PZD Surfaces. The $2n_v$ equality constraints associated with a given partial zero dynamics surface $\mathcal{PZ}_{\alpha_v}$ can be combined with $2(n - n_v)$ additional constraints, such as holonomic constraints, on the state space of the robot to form an inverse kinematics problem with a unique solution $(\vartheta(\alpha_v), \dot{\vartheta}(\alpha_v)) \in \mathcal{PZ}_{\alpha_v}$.

Example 4: (PHZD Reconstruction). In the fully-actuated domain, the states of the system can obtained through PHZD, or simply PZD, reconstruction [1]. This is accomplished by defining,

$$\Phi(\xi_{fa,1}) = \begin{bmatrix} c_{fa} \\ H_{fa} \end{bmatrix}^{-1} \begin{bmatrix} \xi_{fa,1} \\ y^d_{fa,2} \end{bmatrix}, \tag{33}$$

$$\Psi(\xi_{fa,1}) = \begin{bmatrix} c_{fa} \\ H_{fa} \end{bmatrix}^{-1} \begin{bmatrix} 1 \\ \frac{\partial y^d_{fa,2}}{\partial \xi_{fa,1}} \end{bmatrix}.$$

The point $(q, \dot{q}) \in \mathcal{PZ}_{\alpha_v} \cap (\xi_{fa,1}, \xi_{fa,2})$ is found by setting $q = \Phi(\xi_{fa,1})$ and $\dot{q} = \Psi(\xi_{fa,1})\xi_{fa,2}$.

Obtaining PZD Surfaces from States. The extended canonical walking function can be used to create a partial zero dynamics surface connecting any two states. Specifically, for two distinct states: $(\bar{q}, \dot{\bar{q}})$ and $(\hat{q}, \dot{\hat{q}})$, we can solve for α such that $(\bar{q}, \dot{\bar{q}}) \in \mathcal{PZ}_\alpha$ and $(\hat{q}, \dot{\hat{q}}) \in \mathcal{PZ}_\alpha$ using a Motion Transition [10]. In the construction of the optimization problem, Motion Transitions are used to obtain controller parameters for full-actuation, α_{fa}, and under-actuation, α_{ua}.

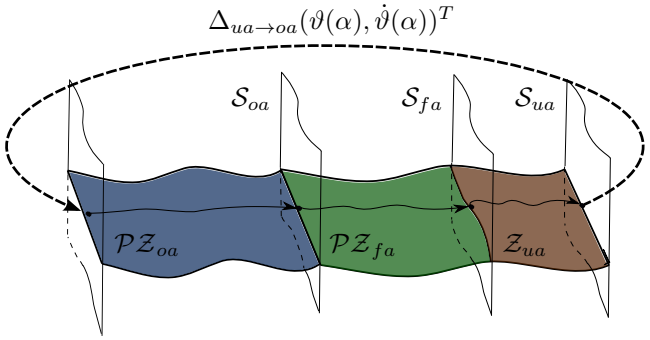

Fig. 4: Geometry of the closed loop obtained using motion transitions.

V. Optimization

The main result of this paper is a method for achieving hybrid invariance across three domains using the properties and usage of partial zero dynamics surfaces described in Section IV. Multi-domain hybrid invariance will be encoded in the form of nonlinear constraints to be solved in an optimization problem.

The Over-Actuated PHZD Surface. To begin the optimization construction, we must first define an additional set of actual outputs $y^a_2(q) := y^H_{2,ua}(q) \in \mathbb{R}^6$ and define corresponding desired outputs $y^d_2(\tau(q), \alpha) := [y_{cwf}(\tau_v(q), \alpha^i_v)]_{i \in O_{ua}}$. Associated with these desired outputs is the matrix α of parameters to be optimized; furthermore, $\alpha_{oa} = (\alpha)_{1,2,3,6,7}$, i.e. the rows in α_{oa} are select rows in α. These additional outputs are not used in control, but they are needed to solve the inverse kinematics problem to obtain a point on the guard of the under-actuated domain.

Let $q^-_{ua} \in S_{ua}$ be the final configuration on the under-actuated domain and $q^+_{oa} = \Delta_q q^-_{ua}$ be the initial configuration in the over-actuated domain. On the surface, $\mathcal{Z}_\alpha$, the angles q^-_{ua} are obtained by solving

$$\vartheta(\alpha) = q^-_{ua} \quad s.t. \quad \begin{bmatrix} y^a_2(\Delta_q q^-_{ua}) - y^d_2(0, \alpha) \\ h_{ua}(\Delta_q q^-_{ua}) \end{bmatrix} = \begin{bmatrix} \mathbf{0}_6 \\ 0 \end{bmatrix}, \tag{34}$$

where $\tau_{oa} = 0$ at the beginning of the over-actuated domain. Using $\vartheta(\alpha)$ and the zero dynamics constraints, $\mathcal{Z}_\alpha$, we can explicitly solve for the velocity vector corresponding to the point $(\vartheta(\alpha), \dot{\vartheta}(\alpha)) \in S_{ua} \cap \mathcal{Z}_\alpha$. The initial state of the over-actuated domain is calculated via $(q^+_{oa}(\alpha), \dot{q}^+_{oa}(\alpha)) = \Delta_{ua\to oa}(\vartheta(\alpha), \dot{\vartheta}(\alpha))$. This quantity is used to compute a *partial hybrid zero dynamics constraint* to be solved in the optimization; this constraint is given by:

$$\Delta_{ua\to oa}(S_{ua} \cap \mathcal{Z}_\alpha) \subset \mathcal{PZ}_{\alpha_{oa}}, \tag{C1}$$

where noting again that $\alpha_{oa} \subset \alpha$, this constraint renders $\mathcal{PZ}_{\alpha_{oa}}$ invariant through impact, $\Delta_{ua\to oa}$. This constraint

can be converted to one that is only a function of α via the construction in [1].

Assuming (C1) is satisfied, the evolution of the robot's state during over-actuation can described by the evolution of the coordinates ξ_{oa}. In particular, associated with the initial state of the over-actuated domain are the initial reduced coordinates state: $\xi_{oa}^+(\alpha) = (\delta p_{hip}(q_{oa}^+(\alpha)), c_{oa}\dot{q}_{oa}^+(\alpha))$ and corresponding solution $\xi_{oa}(t, \xi_{oa}^+(\alpha))$ to (31) and (32). With the goal of forcing a domain transition governed by d_{oa}, we solve for the time T_{oa} corresponding to the end of the domain, i.e. $T_{oa} = \{t : \xi_{oa,1}(t, \xi_{oa}^+(\alpha)) = \xi_{oa,1}^+(\alpha) + d_{oa}\}$ using the Lambert W function as done in [1]. Over the interval $t \in [0, T_{oa}]$ the states of the robot are obtained by solving for $(q_{oa}(t), \dot{q}_{oa}(t)) \in \mathcal{PZ}_{\alpha_{oa}} \cap \xi_{oa}(t, \xi_{oa}^+(\alpha))$; this is done using the method described in Example 4 together with the geometric constraint $\eta_{\text{oa}}(q_{oa}(t)) = 0$. These states can be used to construct constraints on the over-actuated domain

$$\min_{t\in[0,T_{oa})} [\Psi_{oa}(q_{oa}(t), \dot{q}_{oa}(t), u_{oa}^{\alpha_{oa},\varepsilon})] > 0, \qquad \text{(C2)}$$

and a constraint which triggers the guard at $t = T_{oa}$,

$$\Psi_{oa}(q_{oa}(t), \dot{q}_{oa}(t), u_{oa}^{\alpha_{oa},\varepsilon}) = 0. \qquad \text{(C3)}$$

Here, the final state in the over-actuated domain, $(q_{oa}^-(\alpha), \dot{q}_{oa}^-(\alpha)) = (q_{oa}(T_{oa}), \dot{q}_{oa}(T_{oa}))$ is constrained to be on the guard S_{oa} and thus at this point the robot transitions to the fully-actuated domain.

The Fully-Actuated PHZD Surface. The transition map from over-actuation to fully-actuation is used to obtain the initial condition for the fully-actuated domain, i.e. we calculate $(q_{fa}^+(\alpha), \dot{q}_{fa}^+(\alpha)) = \Delta_{oa\to fa}(q_{oa}^-(\alpha), \dot{q}_{oa}^-(\alpha))$. As in the over-actuated domain, associated with the initial state of the fully-actuated domain is the solution $\xi_{fa}(t, \xi_{fa}^+(\alpha))$ to (31) and (32) with initial condition $\xi_{fa}^+(\alpha)$. With the goal of forcing a domain transition governed by d_{fa}, we solve for the time T_{fa} corresponding to the end of the domain, i.e. $T_{fa} = \{t : \xi_{fa,1}(t, \xi_{fa}^+(\alpha)) = \xi_{oa,1}^+(\alpha) + d_{oa} + d_{fa}\}$ again using the Lambert W function as done in [1]. The final states of the robot in the fully-actuated domain are made to satisfy $(q_{fa}^-(\alpha), \dot{q}_{fa}^-(\alpha)) \in \mathcal{Z}_\alpha \cap \xi_{fa}(T_{fa}, \xi_{fa}^+(\alpha))$ via the reconstruction method described in Example 4.

Thus, the initial and final conditions to the fully-actuated domain are $(q_{fa}^+(\alpha), \dot{q}_{fa}^+(\alpha))$ and $(q_{fa}^-(\alpha), \dot{q}_{fa}^-(\alpha))$, respectively. These two points are used to construct a Motion Transition resulting in controller parameters α_{fa}. Over the interval $t \in [0, T_{fa}]$ the states of the robot are obtained by solving for $(q_{fa}(t), \dot{q}_{fa}(t)) \in \mathcal{PZ}_{\alpha_{fa}} \cap \xi_{fa}(t, \xi_{fa}^+(\alpha))$, specifically by using the method described in Example 4. These states can be used to construct constraints on the fully-actuated domain

$$\min_{t\in[0,T_{fa})} \left[\Psi_{fa}(q_{fa}(t), \dot{q}_{fa}(t), u_{fa}^{\alpha_{fa},\varepsilon})\right] > 0. \qquad \text{(C4)}$$

and a constraint which triggers the guard at $t = T_{fa}$,

$$\Psi_{fa}(q_{fa}(t), \dot{q}_{fa}(t), u_{fa}^{\alpha_{fa},\varepsilon}) = 0. \qquad \text{(C5)}$$

Where again, when (C5) is satisfied, the robot transitions to the under-actuated domain as planned.

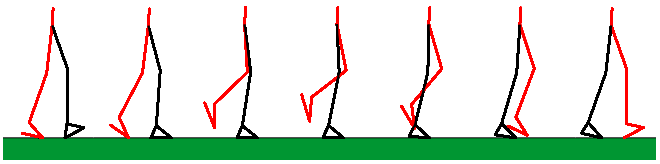

Fig. 5: Snapshots of a three domain walking gait.

The Under-Actuated PHZD Surface. The initial condition to the under-actuated domain is $(q_{ua}^+(\alpha), \dot{q}_{ua}^+(\alpha)) = \Delta_{fa\to ua}(q_{fa}^-(\alpha), \dot{q}_{fa}^-(\alpha))$. Recall that the final condition in this domain is $(\vartheta(\alpha), \dot{\vartheta}(\alpha))$. These two points are used to construct a Motion Transition resulting in controller parameters α_{ua}. As this domain is under-actuated, the states along the surface $\mathcal{Z}_{\alpha_{ua}}$ are obtained through numerical integration of the zero dynamics (as discussed in [25], [1]). As done in the first two domains, constraints are formed to ensure that the states obtained through integration are consistent with the definition of the under-actuated domain:

$$\min_{t\in[0,T_{ua})} [\Psi_{ua}(q_{ua}(t), \dot{q}_{ua}(t), u_{ua}^{\alpha_{ua},\varepsilon})] > 0. \qquad \text{(C6)}$$

In particular, this constraint is satisfied if the solution obtained through numerical integration of this domain reaches $(\vartheta(\alpha), \dot{\vartheta}(\alpha)) \in S_{ua}$.

Main Result: A Multi-Domain PHZD Optimization. With the controllers and constraints defined, the final form of the human inspired, 3-domain optimization becomes,

$$(\alpha^*, d_{fa}^*, d_{ua}^*) = \underset{\alpha, d_{fa}, d_{ua}\in\mathbb{R}^{33}}{\text{argmin}} \ \text{Cost}_{\text{HD}}(\alpha) \qquad \text{(35)}$$
$$s.t. \quad (\text{C1}, \text{C2}, ..., \text{C6})$$

with $\text{Cost}_{\text{HD}}(\alpha)$ the human-data based cost defined in [4]. The solution to (35) is a set of parameters α and transition conditions d_{fa} and d_{ua} corresponding to a hybrid-invariant, three-domain walking gait. Furthermore, the control parameters α_{oa}, α_{fa} and α_{ua} can all be obtained from α.

VI. Simulation Results

This section presents a simulation example showing how the optimization algorithm of Section V was used to produce a multi-domain walking gait for the planar biped AMBER 2, a planar robot that was designed and partially machined within AMBER lab at Texas A&M University. AMBER 2 is a seven link robot supported by a light weight, carbon fiber boom that restricts motion to the saggittal plane. The boom is counter weighted so as to not introduce mass to the robot; however, there is an inertial load introduced to the torso link that is negligible due to the low friction bearings used in the construction of the boom as well as a long moment arm ($\sim$ 8ft) separating the robot from the center of rotation of the boom. The optimization of Section V was implemented using MATLAB's `fmincon` function and the interior-point algorithm. The results of the optimization are shown in Fig. 5, where the three-domain walking gait is plotted as a series of tiles. An animation is available online [13]. The gait shown here has an average velocity of 0.42 m/s, with a step length

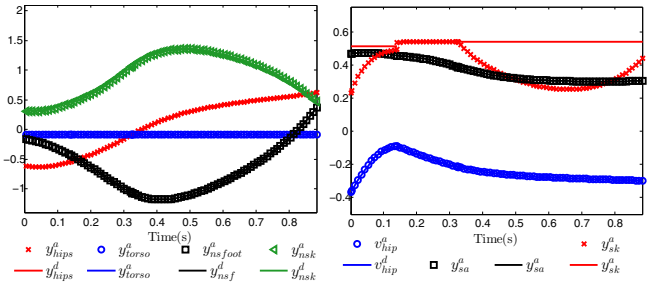

Fig. 6: Actual and desired outputs over one step for a three domain walking gait.

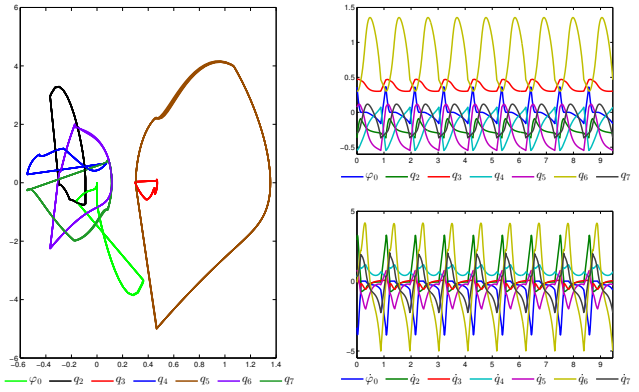

Fig. 7: Phase plot (left) for 9 steps of a 3 domain walking gait showing the periodicity of the gait and joint angles (top right) and velocities (bottom right).

of 0.373 m (58% of leg length) and a period of $T = 0.88$ sec. The step time can be further broken down, with 0.139 s (16%) in over-actuation, 0.19 s (21%) in full-actuation, and 0.56 s (63%) in under-action. The actual and desired outputs are shown in Fig. 6.

VII. Conclusion

The objective of this paper has been to present a novel method with which to design multi-domain walking gaits. The chief contribution lies in the extension of the human-inspired optimization [3] to handle multi-contact locomotion containing both heel strike and toe off. In doing so, it was shown that including motion transitions in the human-inspired optimization allows the robot to remain on the zero dynamics manifold across domains in which the degrees of actuation change. The methods described here have been recently realized on AMBER 2 to achieve robust, multi-domain locomotion experimentally [27], [26].

References

[1] A. D. Ames. Human-inspired control of bipedal walking robots. To appear in IEEE Transactions on Automatic Control, 2014.

[2] A. D. Ames. First steps toward automatically generating bipedal robotic walking from human data. In *Robotic Motion and Control*, volume 422 of *LNICS*, pages 89–116. Springer, 2012.

[3] A. D. Ames, E. A. Cousineau, and M. J. Powell. Dynamically stable robotic walking with NAO via human-inspired hybrid zero dynamics. In *Hybrid Systems: Computation and Control*, 2012.

[4] A. D. Ames, R. Vasudevan, and R. Bajcsy. Human-data based cost of bipedal robotic walking. In *Hybrid Systems: Computation and Control*, Chicago, IL, 2011.

[5] C. Chevallereau, G. Abba, Y. Aoustin, F. Plestan, E. R. Westervelt, C. Canudas-de Wit, and J. Grizzle. Rabbit: a testbed for advanced control theory. *Control Systems, IEEE*, 23(5):57–79, Oct 2003.

[6] J. W. Grizzle, C. Chevallereau, A. D. Ames, and R. W. Sinnet. 3D bipedal robotic walking: models, feedback control, and open problems. In *IFAC Symposium on Nonlinear Control Systems*, Bologna, Italy, 2010.

[7] J. Hurst, J. Grizzle, et al. ATRIAS 2.1 First Steps. `http://youtu.be/uswiqPbFLZ0`.

[8] S. Kagami, K. Nishiwaki, J. J. K. Jr, Y. Kuniyoshi, M. Inaba, and H. Inoue. Online 3d vision, motion planning and bipedal locomotion control coupling system of humanoid robot: H7. In *IEEE Conference on Intelligent Vision Robots and Systems.*, Lausanne Switzerland, Oct. 2002.

[9] S. Kajita, F. Kanehiro, K. Kaneko, K. Fujiwara, K. Harada, K. Yokoi, and H. Hirukawa. Biped walking pattern generator allowing auxiliary ZMP control. In *IEEE/RSJ Intl. Conf. on Intelligent Robots and Systems*, pages 2993–2999, Beijing, P.R. China, 2006.

[10] S. Kolathaya and A. D. Ames. Achieving bipedal locomotion on rough terrain through human-inspired control. In *IEEE International Symposium on Safety, Security, and Rescue Robotics*, College Station, Texas, 2012.

[11] T. Koolen, T. D. Boer, J. Rebula, A. Goswami, and J.Pratt. Capturability-based analysis and control of legged locomotion. part 1: Theory and application to three simple gait models. In *International Journal of Robotics Research*, 2012.

[12] J. Lack. Planar multicontact locomotion using hybrid zero dynamics. Master's thesis, Texas A&M University, College Station, TX, 2013.

[13] J. Lack, M. J. Powell, and A. D. Ames. Planar Multi-Contact Bipedal Walking Using Hybrid Zero Dynamics: Simulation Results. `http://youtu.be/OY-QsaIglQY`.

[14] S.-H. Lee and A. Goswami. Ground reaction force control at each foot: A momentum-based humanoid balance controller for non-level and non-stationary ground. In *International Conference on Intelligent Robots and Systems*, Taipei, Taiwan, 2010.

[15] W. Ma, H. Zhao, S. Kolathaya, A. D. Ames, et al. Robotic Walking with AMBER 2.0. `http://youtu.be/d6oM5sLI9vA`.

[16] J. Pratt, J. Carff, and S. Drakunov. Capture point: A step toward humanoid push recovery. In *in 6th IEEE-RAS International Conference on Humanoid Robots*, Genoa, Italy, 2006.

[17] J. Pratt, T. Koolen, T. D. Boer, J. Rebula, S. Cotton, J. Carff, M. Johnson, and P. Neuhaus. Capturability-based analysis and control of legged locomotion, part 2: Application to m2v2, a lower-body humanoid. In *International Journal of Robotics Research, 2012*, 2012.

[18] M. P. S. Nadubettu Yadukumar and A. D. Ames. Human-inspired underactuated bipedal robotic walking with amber on flat-ground, up-slope and uneven terrain. In *International Conference on Intelligent Robots and Systems*, 2012.

[19] R. Sinnet, M. Powell, R. Shah, and A. D. Ames. A human-inspired hybrid control approach to bipedal robotic walking. In *18th IFAC World Congress*, Milano, Italy, 2011.

[20] R. W. Sinnet and A. D. Ames. 3D bipedal walking with knees and feet: A hybrid geometric approach. In *48th IEEE Conference on Decision and Control*, Shanghai, P.R. China, 2009.

[21] M. W. Spong and F. Bullo. Controlled symmetries and passive walking. *IEEE TAC*, 50(7):1025–1031, 2005.

[22] K. Sreenath, H.-W. Park, and J. Grizzle. Design and experimental implementation of a compliant hybrid zero dynamics controller with active force control for running on mabel. In *Robotics and Automation (ICRA), 2012 IEEE International Conference on*, pages 51–56, May 2012.

[23] T. Takubo, Y. Imada, K. Ohara, Y. Mae, and T. Arai. Rough terrain walking for bipedal robot by using zmp criteria map. In *IEEE Conference on Robotics and Automation.*, Kobe Japan, May 2009.

[24] M. Vukobratović and B. Borovac. Zero-moment point—thirty-five years of its life. *Intl. J. of Humanoid Robotics*, 1(1):157–173, 2005.

[25] E. R. Westervelt, J. W. Grizzle, C. Chevallereau, J. H. Choi, and B. Morris. *Feedback Control of Dynamic Bipedal Robot Locomotion*. CRC Press, Boca Raton, 2007.

[26] H. Zhao, W. Ma, A. D. Ames, et al. Human-Like Multi-Contact Walking with AMBER 2.0. `http://youtu.be/VvkIdCKlL54`.

[27] H. Zhao, W. Ma, M. Zeagler, and A. D. Ames. Human-inspired multi-contact locomotion with AMBER2. To appear in the International Conference on Cyber-Physical Systems, 2014.